Copper Ferrite Nanoparticles Synthesized Using Anion Exchange Resin: Influence of Synthesis Parameters on the Cubic Phase Stability

Svetlana Saikova *, Aleksandr Pavlikov, Denis Karpov, Aleksandr Samoilo, Sergey Kirik, Mikhail Volochaev, Tatyana Trofimova, Dmitry Velikanov, Artem Kuklin

Posted Date: 27 February 2023

doi: 10.20944/preprints202302.0459.v1

Keywords: copper ferrite; magnetic properties; anion-exchange resin precipitation; magnetic nanoparticles

Article

Copper Ferrite Nanoparticles Synthesized Using Anion Exchange Resin: Influence of Synthesis Parameters on the Cubic Phase Stability

Svetlana Saikova [1,2,*], Aleksandr Pavlikov [1], Denis Karpov [1,2], Aleksandr Samoilo [1], Sergey Kirik [1,2], Mikhail Volochaev [3], Tatyana Trofimova [1], Dmitry Velikanov [3] and Artem Kuklin [4]

[1] School of Non-Ferrous Metals and Material Science, Siberian Federal University, 660041 Krasnoyarsk, Russia; ssai@mail.ru (S.S.); hahanka@yandex.ru (A.P.); denikarp@mail.ru (D.K.); x-lab@rambler.ru (A.S.); kiriksd@yandex.ru (S.K.); ttv91@mail.ru (T.T.)

[2] Institute of Chemistry and Chemical Technology, Federal Research Center "Krasnoyarsk Science Center of the Siberian Branch of the Russian Academy of Sciences", 660036 Krasnoyarsk, Russia; ssai@mail.ru (S.S.); denikarp@mail.ru (D.K.); kiriksd@yandex.ru (S.K.)

[3] Kirensky Institute of Physics, Federal Research Center "Krasnoyarsk Science Center of the Siberian Branch of the Russian Academy of Sciences", Akademgorodok, 660036 Krasnoyarsk, Russia; volochaev91@mail.ru (M.V.); dpona1@gmail.com (D.V.)

[4] Department of Physics and Astronomy, Uppsala University, Box 516, SE-751 20 Uppsala, Sweden; artem.icm@gmail.com (A.K.)

* Correspondence: ssai@mail.ru; Tel.: +7-(902)-991-20-31

Abstract: Copper ferrite attracts a lot of interest from researchers as a material with unique magnetic, optical, catalytic and structural properties. In particular, the magnetic properties of this material are structurally sensitive and can be tuned by changing the distribution of Cu and Fe cations in octahedral and tetrahedral positions by controlling synthesis parameters. In this study, we propose a new simple and convenient method for the synthesis of copper ferrite nanoparticles using a strongly basic anion exchange resin in OH form. The effect and possible mechanism of polysaccharides addition on the elemental composition, yield and particle size of $CuFe_2O_4$ is investigated and discussed. It is shown that anion exchange resin precipitation leads to a mixture of unstable at standard temperature cubic (c-$CuFe_2O_4$) and stable tetragonal (t-$CuFe_2O_4$) phases. The effect of the reaction conditions on the c-$CuFe_2O_4$ stability is studied by temperature-dependent XRD measurements and discussed in terms of the cations distribution, Jahn–Teller distortion and Cu^{2+} and oxygen vacancies in the copper ferrite lattice. The obtained differences in the values of saturation magnetization and the coercive force of prepared samples are explained with a reference to variations in the particle sizes and the structural characteristics of copper ferrite.

Keywords: copper ferrite; magnetic properties; anion-exchange resin precipitation; magnetic nanoparticles

1. Introduction

Due to high electric resistance and outstanding magnetic properties, spinel ferrites are excellent candidates for modern technological applications. The copper ferrite nanoparticles (NPs) are being applied in biomedicine (drug delivery [1], magnetic resonance imaging [2], magnetic cell separation, DNA extraction [3]). In addition, they have various technological applications such as energy storage devices [4], magnetic storage media [5], spintronic and electromagnetic devices [6,7]. Besides, ferrites were used as catalysts for photocatalytic degradation of organic matter [8–10], oxidation of dimethyl ether [11] and mercury [12], and reduction of 4-nitrophenol [13]. The spinel structure of ferrites provides additional sites for the catalytic reaction, which leads to an increase in the efficiency of the photocatalytic decomposition [14,15].

 doi:10.20944/preprints202302.0459.v1

Spinels have the general formula [$A^{2+}B^{3+}{}_2O^{2-}{}_4$], where A and B are divalent and trivalent metal cations. Copper ferrite, $CuFe_2O_4$, can be described as a cubic close-packed arrangement of oxygen ions, with Cu^{2+} and Fe^{3+} ions at two different crystallographic sites. These sites have tetrahedral and octahedral oxygen coordination (A and B sites respectively), so the resulting local symmetries of the two sites are different. Depending upon the cation distribution in the lattice, spinels can be divided into normal and inverse. In a normal spinel, tetrahedral sites are occupied by A-cations while octahedral sites are occupied by B-cations. In an inverse spinel, tetrahedral sites are occupied by a half of the B-cations, whereas all A-cations occupy octahedral sites [16,17].

The main method for the industrial production of ferrites remains solid-phase technology, which involves a multi-step careful homogenization of the initial oxides and long-term heat treatment at high temperatures [18]. The sol-gel process proposed in recent years is time-consuming and does not always produce monophase products [19]. Moreover, the resulting particles tend to fuse into large (submicron) particles [20]. Chemical precipitation is the simplest technique; however, the precipitates often capture ions and particles during formation. As the presence of contaminants negatively affects the properties of the resulting materials, so they must be carefully removed, which makes the process more complex and cost-inefective [21].

In this paper, we provide a new approach to produce nano-sized powders of copper ferrite – anion exchange resin precipitation [22]. This technique involves anion exchange between the resin in OH-form and the solution and hydroxides precipitation from the solution. The precipitation is carried out at room temperature and ambient pressure under stable conditions at a constant pH level and can be easily controlled. This makes it possible to obtain particles homogeneous in composition, size and morphology. The particles are also free from impurities and therefore do not require repeated washing and cleaning operations [23–25]. This technique eliminates the need for expensive equipment, provides high yields of products, and ensures low costs, time- and energy-savings. In order to properly tune the growth of the particles and their size and to optimize NPs stability we used polysaccharides with various molar masses and chain structures (dextran-40, dextran-70 and inulin).

An important parameter determining the use of copper ferrite is its crystal structure. It is well-known that copper ferrite can exist in two different structures: tetragonal (t-$CuFe_2O_4$) and cubic (c-$CuFe_2O_4$). t-$CuFe_2O_4$ shows better catalytic activity than c-$CuFe_2O_4$, whereas c-$CuFe_2O_4$ possesses a larger magnetic moment than that of the tetragonal one due to the increased concentration Cu^{2+} at tetrahedral sites [26–29]. t-$CuFe_2O_4$ (space group I41/amd), which is stable at room temperature, forms as a result of the distortion of the cubic lattice of the bulk material in normal conditions. The cubic lattice of c-$CuFe_2O_4$ stretches along a crystallographic structure resulting in the change in the geometry of the unit cell from cubic to tetrahedral. The undistorted cubic structure of copper ferrite (c-$CuFe_2O_4$, space group Fd-3m), in contrast, exists at elevated temperatures – above 440 °C [30]. The unusual behavior of copper ferrite is explained by the d^9-configuration of Cu^{2+} ions leading to removal of degeneracy from the e_g-orbitals (dz^2 and $d(x^2-y^2)$) and the manifestation of the Jahn-Teller effect which reduces the overall symmetry of the system.

According to Ref.[31], coexistence of both phases is possible only in the temperature range of 360-400 °C. In contrast, Yadav et al. [32] revised this statement and emphasized the stability of the cubic phase and coexistence of c-$CuFe_2O_4$ and t-$CuFe_2O_4$, obtained using the sol-gel method, at room temperature. A number of other reports state that structural transformation c-$CuFe_2O_4$→t-$CuFe_2O_4$ is determined by the synthesis conditions. However, despite a considerable amount of research, there is no clear correlation between the used technique and the structure of the copper ferrite. In [20] it is shown that using the sol-gel method tetragonal copper ferrite is formed, whereas the alkaline coprecipitation allows one to obtain c-$CuFe_2O_4$. In contrast, in [33] a cubic modification of copper ferrite was obtained with the use sol-gel method. In addition, to the best of our knowledge, there is no clear explanation for why the cubic structure can remain stable at room temperature instead of transition into the tetragonal phase.

This research aims to explain the effect of polysaccharide additions on the size and structure of copper ferrite particles obtained by the anion exchange resin precipitation method and to shed light

Preprints (www.preprints.org) | NOT PEER-REVIEWED | Posted: 27 February 2023 doi:10.20944/preprints202302.0459.v1

on the structural transition c-$CuFe_2O_4$→t-$CuFe_2O_4$ parameters and reasons for stabilization of cubic phase at room temperature.

2. Materials and Methods

2.1. Chemicals

Copper chloride ($CuCl_2 \cdot 2H_2O$), iron chloride ($FeCl_3 \cdot 6H_2O$), dextran ($(C_6H_{10}O_5)n$ Mr ~40000 Da, ~70000 Da), inulin ($(C_6H_{10}O_5)n$ Mr ~5000 Da) and other chemicals were of analytical grade, were purchased from Sigma-Aldrich and were used as received. The strong-base anion-exchange resin AV-17-8 was produced by "Azot" Corporation (Cherkassy, Ukraine) in the chloride form (AV-17-8(Cl)) with a bead size of 0.4–0.6 mm (Russian GOST 20301-74). This resin is an analogue of Purolite A400/A300, Lewatit M-500, Amberlite IRA 402/420, Dowex SBR-P/Maraton A, it has a gel matrix, based on polystyrene cross-linked with divinylbenzene and the functional group quaternary ammonium (type I). The resin was washed from the monomers by treating it with 1M NaCl solution (volume ratio resin: liquid = 1:3) for 1 hour and then with 2 M NaOH (volume ratio resin: liquid = 1:3 6 more times for 1 hour each to convert it into OH-form (AV-17-8(OH)). The resin was then washed thoroughly with water, dried at the temperature of 60 °C and sieved. The fraction with a bead size >0,5 mm was used in the experiments.

2.2. Synthesis of Copper Ferrite Nanoparticles

In typical experiments, 0,68 g $CuCl_2 \cdot 2H_2O$ and 2,16 g $FeCl_3 \cdot 6H_2O$ were dissolved in 50 mL distilled water or a polysaccharide solution (dextran or inulin) of a given concentration (dextran 40 – 10 weight %, dextran-70 – 6 %, inulin – 30 %). AV-17-8(OH) was added in excess (150 %) to the solution containing copper and ferric salts. The mixture was heated to 60° C and stirred at 180 rpm for 1 hour. To remove the anion-exchange resin beads, a sieve with round holes (0.16 mm in diameter) was used; the precipitate was centrifuged, washed with distilled water, dried in air at 80 °C and then annealed in a muffle furnace at 800 or 900 °C for 1 h.

The resin was also washed with distilled water and then treated three times with 1 M HNO_3 (10 mL portions) while stirring for 1 h. All liquid samples (eluates, stock solutions, dissolved precipitates) were analyzed for copper and iron ions using a Perkin Elmer A Aanalyst 400 Atomic-Absorption spectrometer (USA). The product percent yield (η) and mole fraction of metals in the resin (χ) were defined as the ratio of the total amount of copper and iron moles in the product or eluate to the total amount of the copper and iron moles in the stock solution.

The rate of anion exchange resin precipitation was studied by measuring the ionic conductivities (λ) of reaction solutions on a Multitest KSL-101 (Semico, Novosibirsk, Russia) conductance meter.

2.3. Nanoparticles Characterization

X-Ray powder diffraction data were obtained using an X'Pert PRO diffractometer (PANalytical) with Cu$K\alpha$ radiation. PIXcel (PANalytical), equipped with a graphite monochromator, was used as a detector. The sample was ground in an agate mortar and prepared by the direct cuvette loading method. Scanning conditions: ranged from 3 to 100° on the 2θ scale with a step size of 0.013°, Δt – 50 sec/step, in air at room temperature. High-temperature X-ray studies were carried out by using a HTK1200N (Anton Paar) high-temperature chamber in the air. To prepare the sample about 0.2 g of the substance was loaded into an alumina cuvette. The sample was heated to a certain temperature at a constant rate of 50 °C/min and then scanned within 5 min. Phase identification was carried out using the PDF-2 database card file. Rietveld refinement compositions and cell parameters extraction of obtained materials was carried out in Topas software.

TEM analysis was carried out using a Hitachi 7700M (Hitachi Corporation, Hitachi, Japan, the accelerating voltage: 110 kV). A copper ferrite particle size distribution histogram was obtained from more than 300 particles. The FTIR spectra of samples were recorded on a Tensor 27 (Bruker, Germany) FTIR spectrometer in the range of 4000–400 cm^{-1}.

 doi:10.20944/preprints202302.0459.v1

The magnetic properties of the obtained material were investigated in a magnetic field up to ±15 kOe at 298 K using a vibrating sample magnetometer. An electromagnet with high magnetic field uniformity was used as a source. The magnetic measurements were performed using a direct method of measuring the inductive electromotive force. The mechanical vibrations of the sample were provided by a vibrator of the original design. The relative instability of the oscillation amplitude was 0.01%, with a frequency of 0.001%. The registration of the signal was conducted using the system of four pickup coils. The dynamic range of the device was $5 \cdot 10^{-6}$–10^{2} emu.

3. Results and Discussion

3.1. The Effects of Polysaccharides with Different Molar Masses on the Anion-Exchange Resin Precipitation Process

Copper ferrite nanoparticles were synthesized using an anion exchange resin precipitation process, which can be described by the equation:

$$FeCl_3 + CuCl_2 + 5R\text{-}OH \rightarrow Fe(OH)_3 + Cu(OH)_2 + 5R\text{-}Cl, \quad (1)$$

R-OH and R-Cl are the anion exchange resin AV-17-8 in OH-form and Cl-form.

Anion exchange resin precipitation includes two interconnected chemical reactions. In the first reaction, anions from a solution are exchanged for anions attached to an immobile solid particle:

$$Cl^- + R\text{-}OH \rightarrow OH^- + R\text{-}Cl. \quad (2)$$

The second process is the deposition of metals as insoluble hydroxides

$$Fe^{3+} + Cu^{2+} + 5\ OH^- \rightarrow Fe(OH)_3 + Cu(OH)_2. \quad (3)$$

As the cupric and ferric cations are bounded in their hydroxides and Cl-anions transfer in the sorbent phase, the equilibrium shifts in the direction of the products and the ionic strength and the ionic conductivity of the solution decrease. Reducing the ionic strength of the solution facilitates the production of particles identical in composition and size and containing no impurity ions. The obtained materials have a large surface area and high reactivity [22–25,34].

Deposition of metal hydroxides begins at the resin-solution interface, namely on the resin beads. When the thickness of the surface deposit reaches 1–1.5 μm, it flakes off, and an individual product phase forms [25,31]. The size of the prepared particles can be controlled by the reaction parameters and by the use of stabilizers that prevent agglomeration and aggregation [23].

In this research polyglucan and polyfructan with a molar mass from 5000 to 70000 Da (inulin, dextran-40 and dextran-70) were used to disperse nanoparticles and keep them in a stable colloidal state. Since the solution viscosity affects mass transfer and mass exchange we used polysaccharide solutions with the same kinematic viscosity of 5×10^{-6} m^2/s, which doesn't complicate the resin separation, so the concentrations of the solutions were different for different polysaccharides (dextran-40 – 10 wt. %, dextran-70 – 6 wt. %, inulin – 30 wt. %).

A study of the rate of the anion exchange resin precipitation gave the data shown in Figure 1. The precipitation proceeds fairly quickly in the cases of dextran-40 and inulin additions or without any polysaccharides: the specific electrical conductivity of the reaction solutions is dramatically decreased to zero during 10 min and the extent of the precipitation reached 99 %. At the same time, the addition of dextran-70 drastically reduced the process rate: the precipitation occurred within 60 min. In our opinion, in the presence of dextran-70 a surface deposit with higher adhesive properties on the resin beads has formed, which complicates the diffusion of ions through this layer and reduces the precipitation rate. The deposit flaked away from the resin beads after 30-60 minutes [23,25].

Preprints (www.preprints.org) | NOT PEER-REVIEWED | Posted: 27 February 2023 doi:10.20944/preprints202302.0459.v1

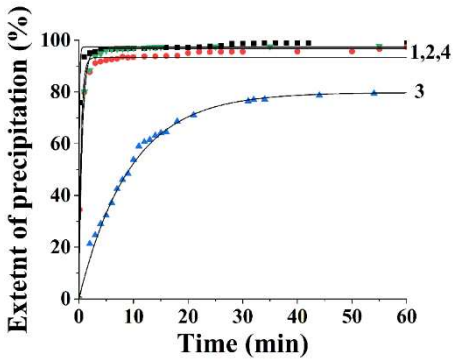

Figure 1. The extent of precipitation of metals as a function of time: 1 – obtained with dextran-40, 2 – obtained with inulin, 3 – obtained with dextran-70, 4 – obtained without polysaccharides.

The elemental composition and yield of the product as well as its phase composition after annealing depends on the type of polysaccharides (polyglucan or polyfructan) and their molar masses (Table 1). XRD (Figure 2) revealed the formation of copper ferrite single-phase structure after annealing at 800 °C for the samples obtained using dextran-40 or inulin and without the polysaccharides. All the diffraction peaks are in good agreement with the JCPDF file for $CuFe_2O_4$ (JCPDF №74-8585 and №34-0425). In the case of the sample with dextran-70, the product contained hematite impurities due to the non-stoichiometry of the precursor. The product yield was only 80 % and the mole fraction of metals in the resin reached 9.8 %. In contrast, in the case of dextran-40 addition, the low metal content in the resin phase (2 %) and the high product yield (98 %) were observed. This might reflect the difference between adhesive properties of the surface precipitates which could be related to the polysaccharide molecules being adsorbed to the nanoparticles. The adsorption of dextran-70 on the nanoparticles as mentioned above prevents the exfoliation of the surface deposit. Conversely, the adsorption of dextran-40 or inulin increases the colloidal stability of nanoparticles and leads to the peptization of the surface deposit.

Table 1. Effect of polysaccharides on the synthesis of copper ferrite and the nanoparticles size.

Sample	Polysaccharide	The mole fraction of metals in the resin, %	The mole ratio of Cu to Fe in the product (n_{Cu}/n_{Fe})	Product yield, %	Average size of nanoparticles (TEM), nm	Phases after annealing
1	-	3.0	0.5[1]	96.0±0.6	134±23	$CuFe_2O_4$
2	Dextran-40	2.0	0.5	98.0±0.6	14±3	$CuFe_2O_4$
3	Dextran-70	9.8	0.4	80.0±1.0	87±24	$CuFe_2O_4$, Fe_2O_3
4	Inulin	2.5	0.5	97.0±0.6	63±14	$CuFe_2O_4$

[1]molar ratio of copper to ferrite 0,5 is stoichiometric for copper ferrite $CuFe_2O_4$.

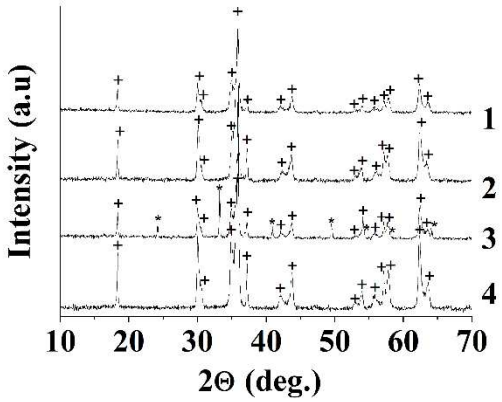

Preprints (www.preprints.org) | NOT PEER-REVIEWED | Posted: 27 February 2023 doi:10.20944/preprints202302.0459.v1

Figure 2. X-ray diffraction patterns of $CuFe_2O_4$ powders annealed at 800 °C: 1 – sample obtained without polysaccharides, 2 – obtained with Dextran-40, 3 – obtained with Dextran-70, 4 – obtained with inulin; + - $CuFe_2O_4$; · - Fe_2O_3.

The adsorption of polysaccharides on the as-prepared samples was confirmed by IR spectroscopy (Figure 3). The absorption bands at 2853 and 2923 cm^{-1} refer to symmetrical and asymmetric vibration of CH_2-groups of polysaccharides. The bands have different intensities that may be attributed to the amount of polysaccharide adsorbed on the nanoparticles. The largest adsorption is observed for the sample obtained using dextran-40 (Figure 3, curve 1). In the case of the sample obtained with dextran-70, the content of the organic phase on the surface of the particles is negligible (Figure 3, curve 3). The adsorbed polysaccharides are completely removed during the annealing of the products at temperatures above 300 °C (Figure 4, Figure S1). The IR spectrum of the powder with dextran-40 additive which was calcined at 800°C for 3 hours consists of only one vibration band at 590 cm^{-1} corresponding to the Fe–O stretching of the ferrite structure (Figure 3, line 5).

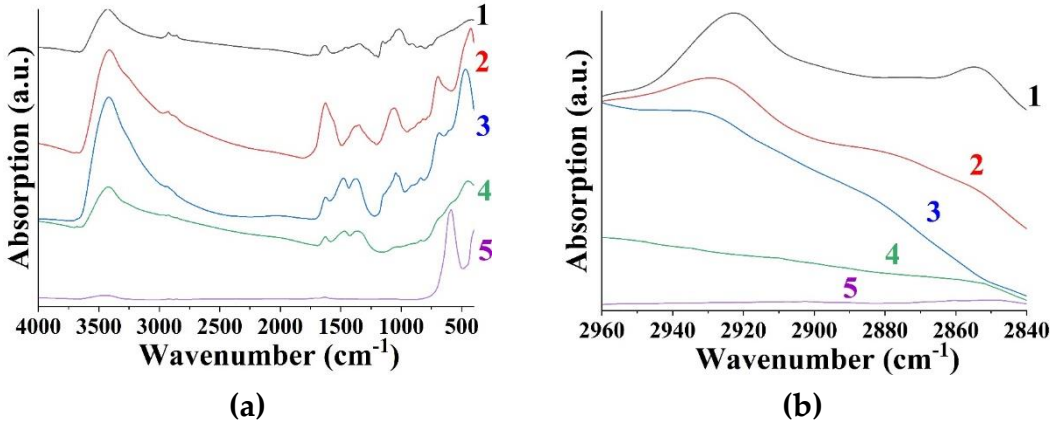

Figure 3. FTIR spectra in the spectral regions of 4000–500 cm^{-1} (a), 2960 – 2840 cm^{-1} (b) of the as prepared samples using dextran-40 (1), inulin(2), dextran-70 (3), without polysaccharides (4) and the sample 2 (table 1) with dextran-40 additive calcined at 800°C (5)

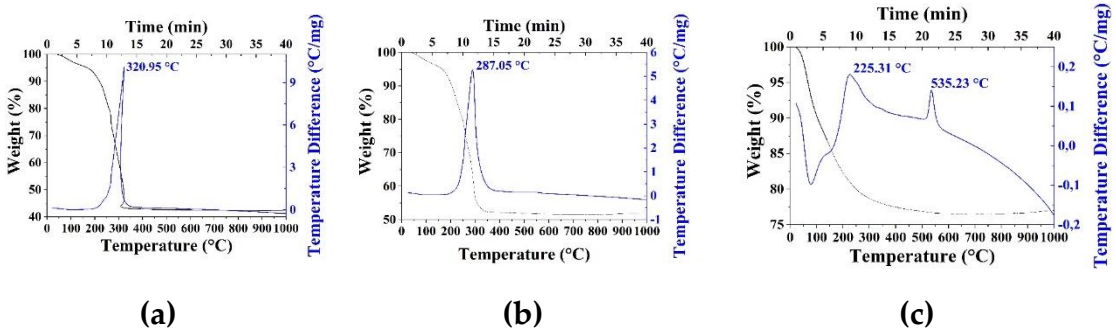

Figure 4. TGA and DSC curves for the as prepared samples with dextran-40 (a), inulin (b) and without polysaccharides (c). The maximums on the DSC curves correspond to complete oxidation of the adsorbed polysaccharide.

The polysaccharides affect the growth process of copper ferrite particles. By adjusting the type and the molar mass of polysaccharides additives we can modify the size of the product. Thus, according to TEM data (Figure 5), the use of dextran with an average molar mass of ~40,000 g/mol led to the formation of copper ferrite nanoparticles with a size of 14±3 nm, while particles of 87± 24 nm were obtained in the presence of dextran-70, and particles with the size of 63 ± 14 nm were synthesized with inulin and particles of 134 nm were produced without any polysaccharides.

The rate of particle aggregation is a major factor that controls the size of crystallites in the final product. When the surface of the colloid adsorbs polysaccharide molecules, the growth rate of the

Preprints (www.preprints.org) | NOT PEER-REVIEWED | Posted: 27 February 2023 doi:10.20944/preprints202302.0459.v1

colloids will be confined and nanoparticle agglomeration will be avoided. Adsorption efficiency is determined by the stability of surface complexes of metal hydroxide with polysaccharides [35]. The binding strength of polysaccharide molecules to the colloid surface depends on the surface area available for binding, the strength of hydrogen bonds and the steric barriers between the polymer molecules. These factors are determined by the molar mass of the polysaccharide and the conformation of its chain: low molar mass polysaccharides are represented by linear chains, while spiral chains formed by medium molar mass polysaccharides and globular are for long-chain molecules. A decrease in the molar mass of the polysaccharide leads to a decrease in the number of bonds and hence a decrease in the stability of the surface complexes. On the other hand, globules that are formed polysaccharides with large molar masses have a small space available for binding with the surface of the particle. Thus, there is an optimum polysaccharide chain length, which, as was noted in Ref. [35], is approximately equal to the length of the circumference of the nanoparticle. The length of the circumference for particles with the size of 14 nm (sample 2, table 1) corresponds to the chain length of a polysaccharide with a molar mass of 40,000 Da. So in this case the most stable colloidal system is formed and particles with a minimum size are produced [23,35]. These results were similar to our previous study, where $CoFe_2O_4$ nanoparticles with a size of 15 nm were obtained in the presence of dextran-40 [36].

The simplicity, time and cost efficiency due to the lack of need for expensive equipment make the proposed method of copper ferrite nanoparticles synthesis convenient, easily reproducible, and scalable under laboratory conditions. In addition, the use of the anion-exchange resin technique makes it possible to obtain an uncontaminated product with reproducible physicochemical properties. The addition of dextran-40 results in the formation of stable colloid dispersions. The high zeta potential of -30.6 mV indicates that the obtained hydrosols are stabilized not only sterically, but also electrically. The resulting nanoparticles can be used as effective catalysts, as well as magnetic nuclei in creation of hybrid "core–shell" nanostructures, which can potentially be applied in biotechnology, nanomedicine and theranostics [37–39].

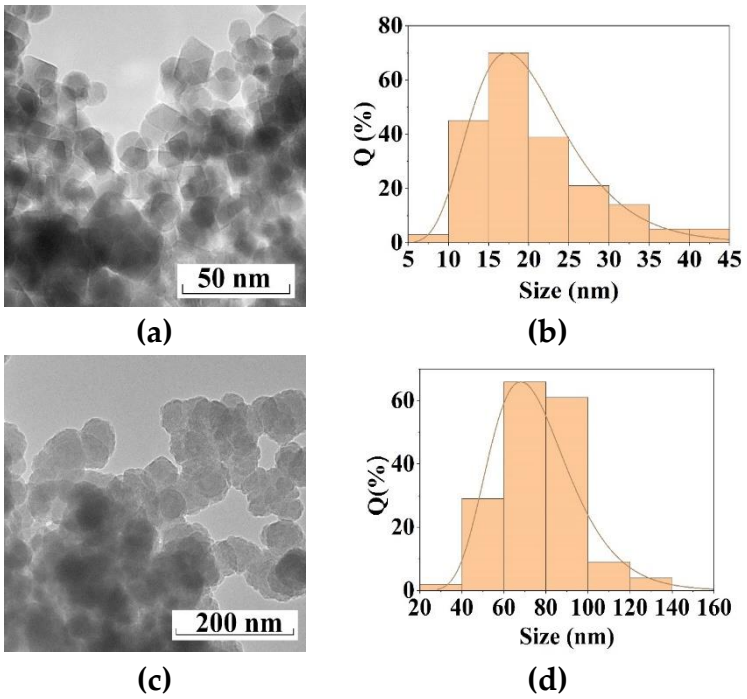

Preprints (www.preprints.org) | NOT PEER-REVIEWED | Posted: 27 February 2023 doi:10.20944/preprints202302.0459.v1

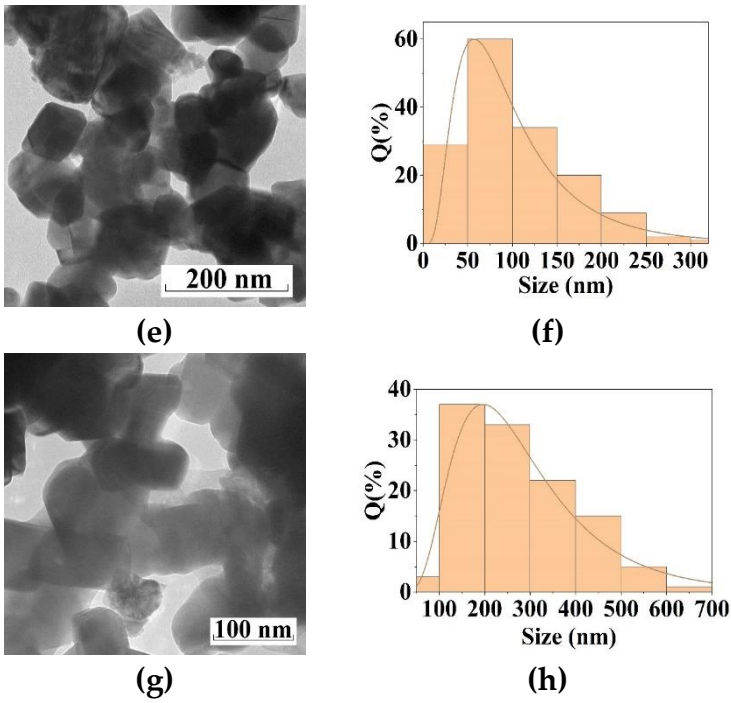

Figure 5. TEM images (left panel) and the particle size distribution diagrams (right panel) for the samples of $CuFe_2O_4$ calcined at 800 °C: (a, b) – obtained with Dextran-40; (c, d) – obtained with inulin; (e, f) – obtained with Dextran-70; (g, h) – obtained without polysaccharides

3.2. Control of Structural Parameters of Copper Ferrite

3.2.1. The Effect of Particle Size on the c-$CuFe_2O_4$ Stability

The important factor that determines the use of copper ferrite is the structure of its crystal lattice. As noted earlier, $CuFe_2O_4$ has a high-temperature cubic modification and a low-temperature tetragonal modification. However, c-$CuFe_2O_4$ can exist at room temperature as well. Several explanations for this phenomenon have been proposed in the literature. Some papers *[40–43]* propose that the main factor in the stability of the cubic modification of copper ferrite is the particle size. The particles <40 nm contribute to the cubic phase stabilization, whereas larger submicron and micron particles lead to the formation of tetragonal copper ferrite. In [44] it was also shown that the particle size significantly affects the temperature of the phase transformation of c-$CuFe_2O_4$→ t-$CuFe_2O_4$, which decreases sharply for 15 nm nanoparticles.

Our results show that although the particle size varied from 14 nm to 134 nm, the change in the cubic phase content was insignificant (22 % to 33 %) and there is no obvious correlation between these values.

Table 2. Cell parameters and phase composition of the samples obtained by ion exchange resin precipitation and annealed at 800°C for 1h.

Sample	Polysaccharide	t-$CuFe_2O_4$ (I41/amd)			c-$CuFe_2O_4$ (Fd-3m)		Fe_2O_3	χ^2
		a	c	ω, wt%	a	ω, wt%	ω, wt%	
1	-	5.853±0.001	8.591±0.001	76±2	8.391±0.001	24±2	-	1.237
2	Dextran-40	5.870±0.001	8.556±0.001	67±2	8.388±0.001	33±2	-	1.413
3	Dextran-70	5.860±0.001	8.581±0.001	56±2	8.385±0.001	22±2	22±2	1.266
4	Inulin	5.857±0.001	8.585±0.001	75±2	8.385±0.001	25±2	-	1.582

Preprints (www.preprints.org) | NOT PEER-REVIEWED | Posted: 27 February 2023 doi:10.20944/preprints202302.0459.v1

Our findings are consistent with the results obtained in papers *[20,43]* where correlation between the dimensional effect and the phase of copper ferrite was not observed. In [43], the sol-gel combustion method was used to obtain c-$CuFe_2O_4$ with the particle size of >100 nm. Submicron particles of stable cubic copper ferrite (Fd-3m) was synthesized under standard conditions by co-precipitation technique [20]. Moreover, the tetragonal phase of copper ferrite may contain small particles too. For example, t-$CuFe_2O_4$ with a particle size of 15-25 nm was reported*[45,46]* .

3.2.2. The Effect of the Annealing Temperature on c-$CuFe_2O_4$ Stability

It is known that copper ferrite is an inverse spinel, which is characterized by the presence of copper ions only in octahedral positions and iron in tetrahedral and octahedral positions. However, some copper ions occupy tetrahedral sites as the result of Cu^{2+} and Fe^{3+} cationic migration. So, a so-called "mixed" spinel is formed, containing Cu and Fe in both tetrahedral (A) and octahedral positions (B) is formed. The resulting distribution of Cu^{2+} and Fe^{3+} ions in this kind of structure can be represented as follows: $(Cu_xFe_{1-x})^A[Cu_{1-x}Fe_{1+x}]^BO_4$, where x is an inversion parameter; if x = 0, the spinel is inverse, and if x = 1, the spinel is normal. A high concentration of Cu^{2+} ions per formula unit in octahedral positions (1-x > 0.8) leads to tetragonal distortion of cubic spinel due to the Jan-Teller effect [47,48].

It has been shown in *[32,49]* that the distribution of cations between tetrahedral and octahedral positions, which is responsible for the evolution of structural phases, increases with rising annealing temperature. In addition, the nonequilibrium distribution of Cu atoms can be maintained at room temperature. In contrast, Refs. *[28,50]* shows that the high annealing temperature contributes to the formation of the tetragonal $CuFe_2O_4$, and the structural change c-$CuFe_2O_4$ → t-$CuFe_2O_4$ occurs when the calcination temperature increases. In the paper [42] cubic copper ferrite was obtained at a temperature below 300 °C whereas a tetragonal phase was produced above 400° C. It is also mentioned that the formation of $CuFe_2O_4$ cubic spinel films is independent of their calcination temperature [51].

We annealed the obtained products at 800 and 900 °C for 1h (Tables 2 and 3). According to the XRD (Figure 5), a mixture of the cubic and tetragonal modifications of copper ferrite with a different mole ratio of c-$CuFe_2O_4$/t-$CuFe_2O_4$ is formed in all the experiments. However, the relative content of cubic phase in samples 2 and 4 increases with temperature rise, and it doesn't change in samples 1 and 3.

Table 3. Cell parameters and phase composition of the samples obtained by ion exchange resin precipitation and annealed at 900°C for 1h.

Sample	Polysaccharide	$CuFe_2O_4$ (I41/amd)			$CuFe_2O_4$ (Fd-3m)		Fe_2O_3	CuO	χ^2
		a	c	ω, wt%	a	ω, wt%	ω, wt%	ω, wt%	
1	-	5.851±0.001	8.596±0.001	78±3	8.390±0.001	22±2	-	-	1.322
2	Dextran-40	5.876±0.001	8.545±0.001	33.6±0.9	8.387±0.001	62.7±0.9	2.3±0.7	1.4±0.3	1.232
3	Dextran-70	5.824±0.001	8.673±0.001	79±1	8.385±0.001	21±1	-	-	1.391
4	Inulin	5.867±0.001	8.558±0.001	60.0±0.8	8.384±0.001	40.0±0.8	-	-	1.594

Preprints (www.preprints.org) | NOT PEER-REVIEWED | Posted: 27 February 2023 doi:10.20944/preprints202302.0459.v1

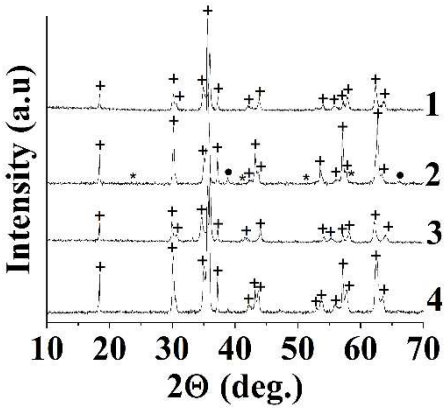

Figure 6. X-ray diffraction patterns of $CuFe_2O_4$ powders annealed at 900 °C: 1 – sample obtained without polysaccharides, 2- obtained with Dextran-40, 3 – obtained with Dextran-70, 4- obtained with inulin; + - $CuFe_2O_4$; * - Fe_2O_3; • - CuO

A detailed study of the evolution of the crystal structure of copper ferrite as a function of temperature was carried out using high-temperature X-ray diffraction. The in situ experiments were carried out on an X'Pert PRO diffractometer (PANalytical) (see Section 2.3) equipped with an HTK1200N high-temperature chamber (Anton Paar). Two samples obtained without polysaccharides and with dextran-40 (1 and 2, table 1) were studied. Heating was carried out from 25°C to 900°C at a rate of 50°C/min. X-ray patterns were recorded every 100 °C. After a 10-minute exposure at 900°C, the sample was cooled to 25°C. Figure 7 presents fragments of X-ray powder patterns in angular range 33 – 37° 2θ corresponding reflection (311) of the c-$CuFe_2O_4$ with the maximum intensity, in the temperature interval of 400 – 900°C .

The samples demonstrate similar behavior when heated. X-ray amorphous powder patterns are observed up to 500 °C (Figure 7). The cubic phase starts to form at 500 °C and is completely formed at 800 °C. The intensity of the main reflection (311) of c-$CuFe_2O_4$ increases with temperature. Sample 2 prepared using dextran-40, crystallizes at a lower temperature. At 900 °C, both samples contain only the cubic phase of copper ferrite. A part of the cubic copper ferrite transforms into a tetragonal modification at cooling. Approximately 47 % of the cubic phase remains in each sample (see Table S1 for Supplementary Materials, Figures S2, S3). The results indicate that the addition of the polysaccharide, as well as the particle size, do not significantly affect the stability of the cubic copper ferrite modification.

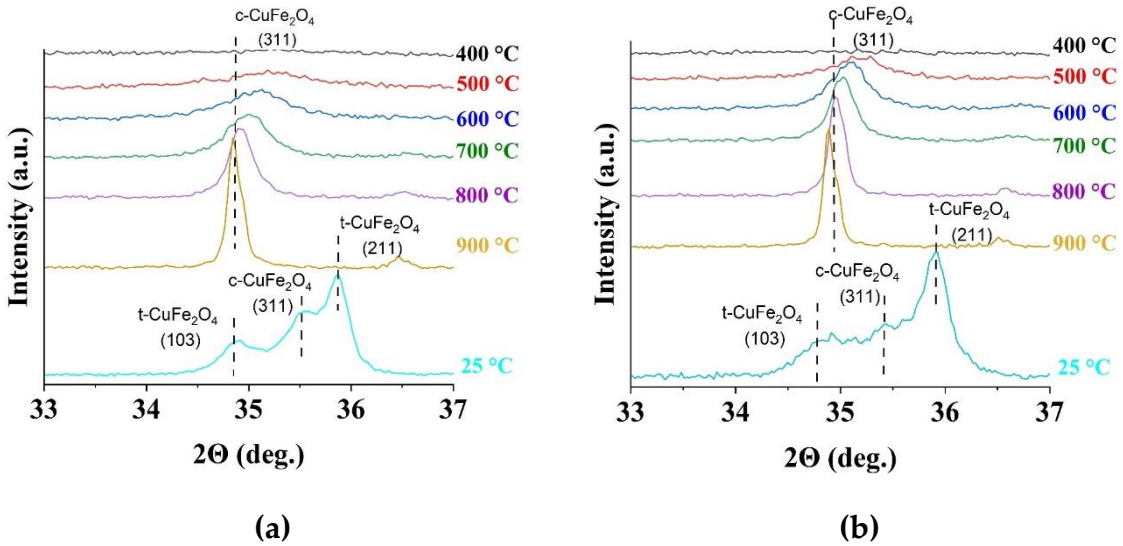

 doi:10.20944/preprints202302.0459.v1

Figure 7. Magnified region of the X-ray diffraction patterns of the as prepared samples 1 and 2 (a – obtained without polysaccharides b – obtained with dextran-40) in the temperature range of 400 – 900 °C with the angular spacing corresponding to the main reflection (311) of the cubic $CuFe_2O_4$.

3.2.3. The Effect of the Cooling Rate on the c-$CuFe_2O_4$ Stability

The chamber for high-temperature X-ray diffraction measurements was cooled by water with a cooling rate of approximately 30 °C/min. Additional experiments with lower and higher cooling rates were conducted on the sample, obtained without polysaccharides (1, Table 1). After being heated up to 900 °C in 30 min with dwell time of 60 min at 900 °C, one sample (indicated as 1f, letter "f" is from 'furnace') remained in the furnace for 7 h until it cooled off to 25 °C and the second one (indicated as 1q, letter "q" is from 'quenching') was removed from the oven and cooled off in room conditions, reaching room temperature in 7 min. The temperature of the samples during cooling time was monitored (Figure S4). The maximum cooling rate was 2.6 and 0.1 °C/s for 1q and 1f samples, respectively, and the cooling decelerated with lower temperatures.

Table 4 and Figure 8, Figure S5, S6 show the phase composition of the samples 1q and 1f and the samples with a non-stoichiometric mole ratio of Cu to Fe: +15 % Cu (Cf and Cq); +15 % Fe (Ff and Fq). Heating and cooling of non–stoichiometric samples were carried out as described above: the samples Cq and Fq were cooled fast (quenched), while the samples Cf and Ff were cooled slowly. Quenching of the samples regardless of their chemical composition leads to a significant increase in relative content of c-$CuFe_2O_4$. These results are in agreement with the literature data *[43,47,48]*. It was shown that the quenching of the samples stabilizes its non-equilibrium high-temperature state where copper cations with an equal probability are distributed between tetrahedral and octahedral lattice positions. Alternatively, furnace cooling is slow enough to establish the equilibrium distribution of Cu resulting in tetragonal distortion [51].

Table 4. Phase composition of the samples with different mole ratios of Cu to Fe annealed at 900 °C and cooled at various rates.

Sample	Mole ratio n(Cu)/n(Fe)	Cooling mode	ω(t-$CuFe_2O_4$), %	ω(c-$CuFe_2O_4$), %	ω(CuO), %	χ^2
1f	0,5	In furnace	81±2	16±2	3.0±0.2	1.449
1q		Quenching	67±1	29±1	4.0±0.3	1.358
Cf	0,6	In furnace	79 ±2	14±2	7.0±0.4	1.439
Cq		Quenching	68±1	23±1	9.0±0.4	1.339
Ff	0,4	In furnace	84±2	16 ±1	-	1.506
Fq		Quenching	55±1	44 ±1	1.0±0.3	1.289

3.2.4. The Effect of Elemental Composition on the c-$CuFe_2O_4$ Stability

Most of the investigated samples, regardless of their mole ratio n(Cu)/n(Fe), contain monoclinic CuO as a second phase (Table 4), even in the case of 15 % excess of iron (sample Fq). At the same time, separate iron oxide phase was not detected (Figure 8). The amount of CuO correlates with the relative content of the cubic copper ferrite, in good agreement with the known results [20,52,53]. We believe that CuO is formed during the cooling of c-$CuFe_2O_4$ and stabilizing the cubic modification. Table S1 and Figure S2,S3 represent the phase composition of samples 1 and 2 (Table 1), determined at 900 °C during high-temperature X-ray diffraction measurements and after cooling to 25 °C. c-$CuFe_2O_4$ is the only phase observed at high temperatures. During the cooling process, the cubic peaks are reduced, and a doublet, corresponding to the tetragonal phase as well as the peaks corresponding to CuO appear. It is noted that the formation of CuO occurs during the thermal decomposition of $CuFe_2O_{4-\delta}$ in the temperature range 900-1100 °C [54]:

 doi:10.20944/preprints202302.0459.v1

$$CuFe_2O_{4-\delta} = 4\delta Cu_{0.5}Fe_{2.5}O_4 + (1-5\delta)CuFe_2O_4 + 3\delta CuO \quad (4)$$

The composition $CuFe_2O_{4-\delta}$ corresponds to the non-stoichiometric oxygen-deficient copper ferrite, which formed due to the loss of oxygen during high-temperature heat treatment of the precursors [48]. Oxygen deficiency is represented by oxygen vacancies, and the value of δ varies depending on the partial pressure of oxygen and the temperature of heating. The oxygen loss is followed by partial reduction of Cu^{2+} to Cu^{+} [32]. Further, when the ferrite is cooled, secondary oxidation leads to the segregation of tenorite CuO and the formation of copper ferrite with a copper deficiency and an excess of iron - $Cu_{1-\eta}Fe_{2+\eta}O_4$, where η varies in a wide range from 0.04 to 0.5. These deviations from stoichiometry are typical of cubic copper ferrite *[54–56]*. We suppose that the formation of copper ferrite with excess (superstoichiometric) iron is the reason for the lack of a separate phase of iron oxides in the samples Ff and Fq. These changes in composition during annealing initiate the transition of Cu^{2+} from octahedral to tetrahedral positions. Thus, the stabilisation of the cubic phase is not only caused by the migration of Cu^{2+} but also related to the change in the oxygen content. The oxygen diffusion depends on the high-temperature treatment duration of copper ferrite, that is not addressed in many studies and may be the cause of controversial results reported previously.

It should be noted that the loss of oxygen during heating may be irreversible in the case of quenching of the samples or it may occur reversibly at a low cooling rate. Quenching of the $CuFe_2O_4$ stabilizes as Cu^{2+} at tetrahedral sites well as oxygen and copper vacancies in the crystal lattice. These processes are responsible for the stability of the non-stoichiometric phase of cubic copper ferrite at room temperature. The excess of iron ions in the precursor also contributes to this effect. The synergies of these factors are illustrated by the Fq sample (Table 4), for which the maximum content of c-$CuFe_2O_4$ is observed.

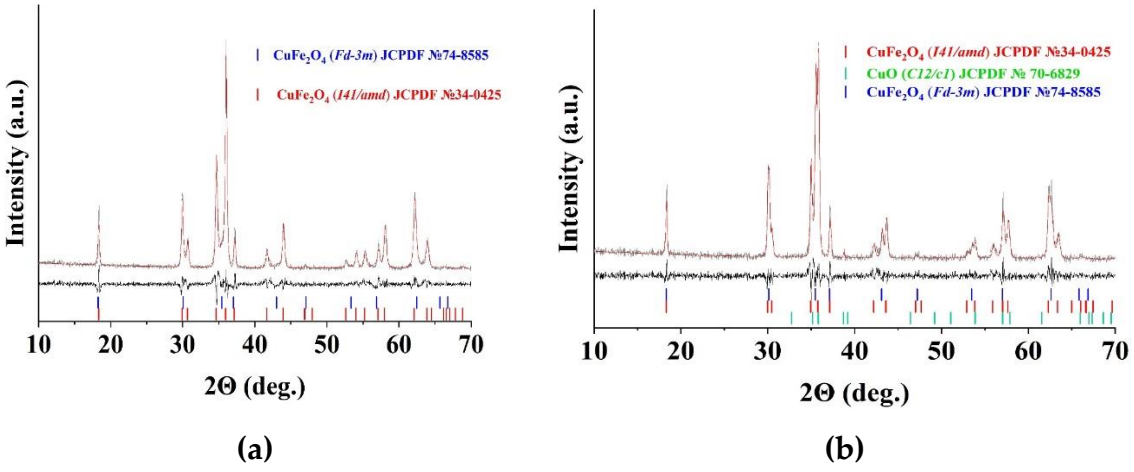

Figure 8. Phase composition of samples Ff (a) and Fq (b). The red line indicates the calculated model. The difference between both values and the line diagram of phases (c-$CuFe_2O_4$, t-$CuFe_2O_4$, CuO) are presented in the lower portion of the graph.

3.3. The Effect of the $CuFe_2O_4$ Nanoparticles Structure on Their Magnetic Properties

Figure 9 shows the dependence of the magnetization of the $CuFe_2O_4$ nanoparticles obtained without polysaccharides and with dextran-40 (samples 1 and 2, Table 1) on the applied magnetic field measured at 298 K. The values of the saturation magnetization (Ms) were estimated in magnetic field H = ±15 kOe. The specific residual magnetizations (Mr) were determined from the point of intersection of the drop-down portion of the magnetization curve with the Y-axis. The values of coercivity (Hc) of the nanoparticles were determined by the measurement of the hysteresis loop width. The basic parameters of the hysteresis loops are collected in Table 5.

The observed saturation magnetization (Ms) value of sample 2 is slightly higher than that of sample 1 due to the larger amount of cubic phase. Both samples demonstrate typical ferrimagnetic

Preprints (www.preprints.org) | NOT PEER-REVIEWED | Posted: 27 February 2023 doi:10.20944/preprints202302.0459.v1

behavior. Since the magnetic moments of copper (II) ions (1.73 μB) and iron (III) ions (5.92 μB) differ greatly, the magnetic properties of $CuFe_2O_4$ strongly depend on the distribution of cations in octahedral and tetrahedral positions [37]. The total magnetic moment (μ) at ferrimagnetic configurations $(Cu_xFe_{1-x})^A[Cu_{1-x}Fe_{1+x}]^BO_4$ can be calculated by a formula

$$\mu = \mu Cu + 2x(\mu Fe - \mu Cu), \quad (4)$$

where μFe and μCu are the magnetic moments of ions Fe^{3+} and Cu^{2+}. This formula shows that the total magnetic moment increases when the amount of copper ions in tetrahedral positions increases, which is typical for c-$CuFe_2O_4$.

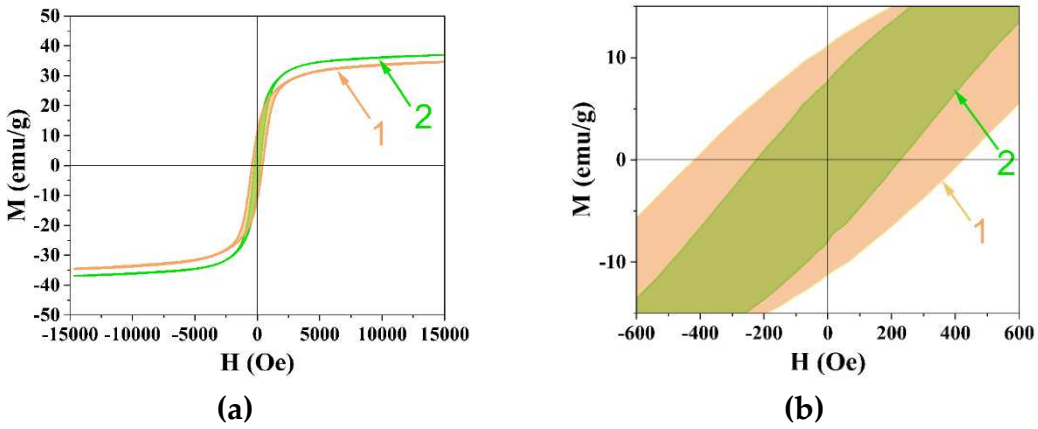

Figure 9. The magnetization curves (a) and their partial enlarged detail (b) measured in magnetic field H =±15kOe at 298 K: 1 - without the use of polysaccharides and 2- using dextran-40.

Table 5. Magnetic parameters obtained from the results of magnetic hysteresis loops in Figure 9.

Sample	Polysaccharide	c-$CuFe_2O_4$/ t-$CuFe_2O$	Ms, emu/g	Mr,emu/g	Hc, Oe	Size of nanoparticles (TEM), nm
1	-	0.3	34.6	10.6	417.0	134±23
2	Dextran-40	0.6	36.9	6.8	220.0	14±3

The observed Ms values of samples 1 and 2 are close to each other and noticeably lower than the bulk value of t-$CuFe_2O_4$ (74.1 emu/g) [57,58]. It is known that the value of Ms decreases with decreasing crystallite size. Such behavior of the nanocrystalline samples could be associated to the large surface area of the nanoparticles that leads to significant adsorption of impurity atoms on the surface and the structural disorder of surface atoms [41]. Since the particle size of sample 2 is much smaller (14±3 nm) than that of sample 1 (134±23), its saturation magnetization should be significantly lower. However, along with the particle size decrease, the ratio c-$CuFe_2O_4$/t-$CuFe_2O_4$ increases, and leads to an increase in the net saturation magnetization value. Thus, the size effect and the cationic disordering effect are acting in opposite directions leading to the values Ms being relatively equal for both samples.

By contrast, the coercive force (Hc) values of the samples differ significantly. As a rule, the coercivity of magnetic nanomaterials is very sensitive to size variation and decreases to zero with decreasing particle size when the magnetic multi-domain state converts to a single-domain state and the particle enters the superparamagnetic regime [59]. The ferromagnetic-to-superparamagnetic transition in $CuFe_2O_4$ nanoparticles is not only due to the size effect. The coercivity increases with structural transformation c-$CuFe_2O_4$→t-$CuFe_2O_4$ due to the large anisotropy arising from the tetragonal distortion [51].

Thus, the magnetic properties of the copper ferrite nanoparticles depend on their structural characteristics and can be tuned by varying the reaction parameters (the mole ratio of the reactants used in the reaction, temperature and time for heat treatment process, the cooling rate, etc.). These

conditions vary from paper to paper, that may explain the diversity of the obtained results. Some of these conditions are often not properlly managed, that may explain why the experimental results obtained in different research papers do not correlate to each other. At the same time, the measured here magnetic parameters of copper ferrite nanoparticles are in agreement with those reported elsewhere: Ms = 31.4 emu/g, Hc = 400.3 Oe, [19], Ms = 27.4 emu/g Hc = 526.6 Oe [20], Ms = 41.1 emu/g Hc = 241 Oe [60], Ms = 32.4 emu/g, Hc = 517 Oe [61].

4. Conclusions

In this paper, a new cost-, time- and energy-efficient technique using anion exchange resin in OH form as a reaction agent has been proposed to obtain homogeneous copper ferrite nanoparticles with uniform size and morphology without any impurity ions. The technique does not require expensive equipment and ensures a high yield of product. The addition of polysaccharides of the different molar masses and chain structures during precipitation significantly influences the growth and agglomeration of particles. The use of inulin with an average molar mass of 5 kDa led to the formation of the particles with a size of 63 ±14 nm; in the presence of dextran (70 kDa), the particles with a size of 87 ±24 nm were obtained; the use of dextran (40 kDa) results in particles of14 ± 3 nm; absence of polysaccharides leads to the particles with a size fo 134 ± 23 nm. Our high-temperature XRD study has shown that a significant part of cubic copper ferrite formed at 500 °C remains stable at the room temperature. We examined possible causes of the stability of the unstable $CuFe_2O_4$ cubic modification and established that there is no significant effect of polysaccharide additives, the particle size, or the annealing temperature in the range of 800-950 °C. We demonstrated that the relative content of cubic phase in the samples noticeably increases when the samples are cooled fast in the air (quenched) and when there is an excess of iron ions in the precursors. These factors contribute to the formation of oxygen and Cu^{2+} vacancies in the ferrite crystal lattice and the cation distribution, which result in stabilization of the non-equilibrium state of copper ferrite. Despite the structural sensitivity of the $CoFe_2O_4$ magnetic properties, we did not find significant differences in the values of saturation magnetization and residual magnetization for the samples with the different content of cubic phases because of large differences in particle size in the samples (14 and 134 nm). However, the coercivity values of the samples differ nearly twice due to the size effect and the magnetic anisotropy from the tetragonal distortion. We believe it is possible to tune the magnetic properties of copper ferrite for its use in various applications by controlling the reaction parameters for magnetic and microwave and biomedical applications.

Supplementary Materials: The following supporting information can be downloaded at the website of this paper posted on Preprints.org. Figure S1: Optical absorption spectra of gases evolved during TGA (thermal decomposition oforganic part; Table S1: Phase composition of samples 1 and 2 (tabl.1) obtained by ion exchange resin precipitation after XRD high-temperature measurements at 900 ° C and after cooling to 25°C; Figure S2: X-ray diffraction patterns of samples 1 and 2 at 900 °C ; top graph – obtained without polysaccharides, bottom graph – obtained with dextran-40. + - cubic $CuFe_2O_4$ (Fd-3m); * - Pt (Platinum); Figure S3: X-ray diffraction patterns of samples 1 and 2 after cooling from 900 °C to 25 °C at a rate of ~30 °C/min; top graph – obtained without polysaccharides, bottom graph – obtained with dextran-40. + - $CuFe_2O_4$; • - CuO; Figure S4: The temperature of the samples as a function of time: a – quenching; b – cooling in the furnace; Figure S5: Rietveld refinement of XRD pattern of samples Cf (a) and Cq (b) where solid curve (grey line) is the observed data and solid curve (red line) is the best fit, vertical marks indicate the Bragg peaks, and the bottom curve shows the difference between observed and calculated intensities.; Figure S6: Rietveld refinement of XRD pattern of samples 1f (a) and q (b) where solid curve (grey line) is the observed data and solid curve (red line) is the best fit, vertical marks indicate the Bragg peaks, and the bottom curve shows the difference between observed and calculated intensities..

Author Contributions: Conceptualization, S.S., A.P., T.T. and D.K.; formal analysis, A.S., S.S., A.P., T.T., D.K.; investigation, A.P., T.T., S.K., D.K., M.V., A.S. and D.V.; methodology, S.S.; supervision, S.S.; validation, S.S.; writing—original draft, S.S., A.P. and T.T.; writing—review and editing, S.S., S.K., A.K. All authors have read and agreed to the published version of the manuscript.

Funding: The Russian team acknowledges the support of Russian Science Foundation (Project 22-73-10047).

Institutional Review Board Statement: Not applicable.

Informed Consent Statement: Not applicable.

Data Availability Statement: Not applicable.

Acknowledgments: This research was partially carried out using the equipment of Krasnoyarsk Regional Center of Research Equipment of Federal Research Center "Krasnoyarsk Science Center SB RAS".

Conflicts of Interest: The authors declare no conflict of interest. The funders had no role in the design of the study; in the collection, analyses, or interpretation of data; in the writing of the manuscript; or in the decision to publish the results.

References

1. Mohamed, I.A.A.M.; Mohamed, M.G.;, Ahmad, S. K.;Ramy, A. F.; Ahmed, I.O.;Ala'a H. Al-M.; David, W. R.; Mohamed, A. M.;Norhan, N.; Ahmed, H. A. Insights on magnetic spinel ferrites for targeted drug delivery and hyperthermia applications. *Nanotechnology Reviews* **2022**, *11*, 372-413.
2. Avasthi, A.; Caro, C.;Pozo-Torres, E.; Leal, M. P.; García-Martín, M. L. Magnetic Nanoparticles as MRI Contrast Agents. Topics in Current Chemistry. *Surface-modified Nanobiomaterials for Electrochemical and Biomedicine Applications* **2020**, *378*,49-91.
3. Nam, J.-H.;Joo, Y.-H.; Lee, J.-H.; Chang, J. H.; Cho, J. H.; Chun, M. P.; Kim, B. I. Preparation of NiZn-ferrite nanofibers by electrospinning for DNA separation. *Journal of Magnetism and Magnetic Materials* **2009**, *321*, 1389–1392.
4. Raut, S. D.;Sangale, S.; Mane, R. S. Ferrites in energy. Spinel Ferrite Nanostructures for Energy Storage Devices. *Elsevier* **2020**, 173–187. doi:10.1016/b978-0-12-819237-5.00008-0
5. Huang, W.; Zhu, J.; Zeng, H. Z.; Wei, X. H.; Zhang, Y.; Li, Y. R. Strain induced magnetic anisotropy in highly epitaxial CoFe2O4 thin films. *Applied Physics Letter s***2006**, *89*, 262506.
6. Pardavi-Horvath, M. Microwave applications of soft ferrites. *Journal of Magnetism and Magnetic Materials* **2000**, *215*,171–183.
7. Carey, M. J.; Maat, S.; Rice, P.; Farrow, R. F. C.; Marks, R. F.; Kellock, A.; Gurney, B. A. Spin valves using insulating cobalt ferrite exchange-spring pinning layers. *Applied Physics Letters* **2002**, *81*, 1044–1046.
8. Kubacka, A.; Fernández-García, M.; Colón, G. Advanced Nanoarchitectures for Solar Photocatalytic Applications. *Chemical Reviews* **2011**, 112, 1555–1614.
9. Shen, Y.; Wu, Y.; Xu, H.; Fu, J.; Li, X.; Zhao, Q.; Hou, Y. Facile preparation of sphere-like copper ferrite nanostructures and their enhanced visible-light-induced photocatalytic conversion of benzene. *Materials Research Bulletin* **2013**, *48*, 4216–4222.
10. Vosoughifar, M. Preparation and application of copper ferrite nanoparticles for degradation of methyl orange. *Journal of Materials Science: Materials in Electronics***2016**, *27*, 10449–10453.
11. Smyrnioti, M.; Ioannides, T. Dimethyl Ether Oxidation over Copper Ferrite Catalysts. *Catalysts* **2022**, 12, 604.
12. Yang, Y.; Liu, J.; Wang, Z.; Ding, J.; Yu, Y. Charge-distribution modulation of copper ferrite spinel-type catalysts for highly efficient Hg^0 oxidation. *Journal of Hazardous Materials* **2020**,*402*, 123576.
13. Hou, C.; Zhao, D.; Chen, W.; Li, H.; Zhang, S.; Liang, C. Covalent Organic Framework-Functionalized Magnetic $CuFe_2O_4$/Ag Nanoparticles for the Reduction of 4-Nitrophenol. *Nanomaterials* **2020**, *10*, 426.
14. Dom, R.; Subasri, R.; Radha, K.; Borse, P. H. Synthesis of solar active nanocrystalline ferrite, MFe_2O_4 (M: Ca, Zn, Mg) photocatalyst by microwave irradiation. *Solid State Communications* **2011**, *151*, 470–473.
15. Peymanfar, R.; Ramezanalizadeh, H. Sol-gel assisted synthesis of $CuCr_2O_4$ nanoparticles: An efficient visible-light driven photocatalyst for the degradation of water pollutions. *Optik* **2018**, *169*, 424–431.
16. Ziemniak,S.E.;Gaddipati, A.R.; SanderP.C. Immiscibility in the $NiFe_2O_4$–$NiCr_2O_4$ spinel binary, *Journal of Physics and Chemistry of solids* **2005**, *66*, 1112–1121.
17. Wang, Z.; Saxena, S.;Lazor, P.; O'Neill, H. S. An in situ Raman spectroscopic study of pressure induced dissociation of spinel $NiCr_2O_4$. *Journal of Physics and Chemistry of Solids* **2003**, *64*, 425–431.
18. Shaheen, W. M.; Ali, A. A. Thermal solid–solid interaction and physicochemical properties of CuO–Fe2O3 system. *International Journal of Inorganic Materials* **2001**,*3*, 1073–1081.
19. Calvo-de la Rosa, J.; Segarra, M. Optimization of the Synthesis of Copper Ferrite Nanoparticles by a Polymer-Assisted Sol–Gel Method. *ACS Omega* **2019**, *4*, 18289–18298.
20. Calvo-de la Rosa, J.; Segarra Rubí, M. Influence of the Synthesis Route in Obtaining the Cubic or Tetragonal Copper Ferrite Phases. *Inorganic Chemistry* **2020**, *59*, 8775-8788.
21. Salavati-Niasari, M; Mahmoudi, T.;Sabet, M.;Hosseinpour-Mashkani, S. M.;Soofivand, F.;Tavakoli, F. Synthesis and Characterization of Copper Ferrite Nanocrystals via Coprecipitation. *Journal of Cluster Science* **2012**, *23*, 1003–1010.
22. Trofimova, T. V.; Saikova, S. V.; Panteleeva, M. V.;Pashkov, G. L.;Bondarenko, G. N. Anion-Exchange Synthesis of Copper Ferrite Powders. Glass and Ceramics **2018**,*75*, 74–79.

23. Saikova, S. V.; Trofimova, T. V.;Pavlikov, A. Y.;Samoilo, A. S. Effect of Polysaccharide Additions on the Anion-Exchange Deposition of Cobalt Ferrite Nanoparticles. *Russian Journal of Inorganic Chemistry* **2020**, *65*,291–298.
24. Ivantsov, R.;Evsevskaya, N.;Saikova, S.; Linok, E.;Yurkin, G.; Edelman, I. Synthesis and characterization of $Dy_3Fe_5O_{12}$ nanoparticles fabricated with the anion resin exchange precipitation method. *Materials Science and Engineering: B* **2017**, *226*,171–176.
25. Evsevskaya, N.; Pikurova, E.; Saikova, S. V.; Nemtsev, I. V. Effect of the Deposition Conditions on the Anion Resin Exchange Precipitation of Indium(III) Hydroxide. *ACS Omega* **2020**, *5*, 4542–4547.
26. Nikolić, V. N.;Vasić, M. M.; Kisić, D. Observation of c-CuFe2O4 nanoparticles of the same crystallite size in different nanocomposite materials: The influence of Fe3+ cations. Journal of Solid State Chemistry **2019**,275, 187–196.
27. Ponhan, W.; Maensiri, S. Fabrication and magnetic properties of electrospun copper ferrite (CuFe2O4) nanofibers. *Solid State Sciences* **2009**, *11*, 479–484.
28. Xiao, Z., Jin, S., Wang, X., Li, W., Wang, J., Liang, C. Preparation, structure and catalytic properties of magnetically separable Cu–Fe catalysts for glycerol hydrogenolysis. *Journal of Materials Chemistry* **2012**, *22*, 16598.
29. Teraoka, Y.; Kagawa, S. Simultaneous catalytic removal of NO_x and diesel soot particulates. *Catalysis Surveys from Japan* **1998**, *2*, 155–164.
30. Balagurov, A. M.;Bobrikov, I. A.;Maschenko, M. S.;Sangaa, D.; Simkin, V. G. Structural phase transition in $CuFe_2O_4$ spinel. *Crystallogr. Rep.* **2013**, *58*, 710–717.
31. Balagurov, A. M.;Bobrikov, I. A.;Pomjakushin, V. Y.; Sheptyakov, D. V.;Yushankhai, V. Y. Interplay between structural and magnetic phase transitions in copper ferrite studied with high-resolution neutron diffraction. *Journal of Magnetism and Magnetic Materials* **2015**, *374*, 591–599.
32. Yadav, R. S.;Havlica, J.;Masilko, J.;Kalina, L.;Wasserbauer, J.;Hajdúchová, M.;Enev,V.; Kuřitka, I.; Kožáková, Z. Cation Migration-Induced Crystal Phase Transformation in Copper Ferrite Nanoparticles and Their Magnetic Property. *Journal of Superconductivity and Novel Magnetism***2015**, *29*, 759–769.
33. López-Ramón, M. V.; Álvarez, M. A.; Moreno-Castilla, C.;Fontecha-Cámara, M. A.;Yebra-Rodríguez, Á.; Bailón-García, E. Effect of calcination temperature of a copper ferrite synthesized by a sol-gel method on its structural characteristics and performance as Fenton catalyst to remove gallic acid from water. *Journal of Colloid and Interface Science* **2018**, *511*, 193–202.
34. Saikova. S.V.; Kirshneva, E.A.; Panteleeva, M.V.; Pikurova, E.V.; Evsevskaya, N.P. Production of Gadolinium Iron Garnet by Anion Resin Exchange Precipitation. *Russian Journal of Inorganic Chemistry* **2019**, *64*, 1191-119.
35. Nikolic, G. S.;Cakic, M. D. Physical investigation of the colloidal iron-inulin complex. *Colloid Journal***2007**, *69*, 464–473
36. Saikova, S.; Pavlikov, A.; Trofimova, T.; Mikhlin, Y.; Karpov, D.; Asanova, A.; Grigoriev, Y.; Volochaev, M.; Samoilo, A.; Zharkov, S.; Velikanov, D. Hybrid Nanoparticles Based on Cobalt Ferrite and Gold: Preparation and Characterization. *Metals* **2021**, *11*, 705
37. Atacan, K. CuFe2O4/reduced graphene oxide nanocomposite decorated with gold nanoparticles as a new electrochemical sensor material for L-cysteine detection. Journal of Alloys and Compounds **2019**, *791*, 391–401.
38. Jermy, B. R., Ravinayagam, V., Alamoudi, W. A., Almohazey, D., Dafalla, H., Hussain Allehaibi, L., Bayka, A.; Toprak, M.S.; Somanathan, T. Targeted therapeutic effect against the breast cancer cell line MCF-7 with a CuFe2O4/silica/cisplatin nanocomposite formulation. *Beilstein Journal of Nanotechnology* **2019**, *10*, 2217–2228.
39. Ahamed, M.; Akhtar, M. J.;Alhadlaq, H. A.;Alshamsan, A. Copper ferrite nanoparticle-induced cytotoxicity and oxidative stress in human breast cancer MCF-7 cells. *Colloids and Surfaces B: Biointerfaces* **2016**, *142*, 46–54.
40. Chatterjee, B. K.; Bhattacharjee, K.; Dey, A.; Ghosh, C. K.; Chattopadhyay, K. K. Influence of spherical assembly of copper ferrite nanoparticles on magnetic properties: orientation of magnetic easy axis. *Dalton Trans.* **2014**, *43*, 7930–7944.
41. Roy, S.; Ghose, J. Superparamagnetic nanocrystalline $CuFe_2O_4$. *Journal of Applied Physics* **2000**, *87*,6226–6228.
42. Yokoyama, M.; Nakamura, A.; Sato, T.; Haneda, K.Jahn-Teller effect in ultrafine copper ferrite particles. *Journal of The Magnetics Society of Japan***1998**,*22*, 243–245.
43. Zhuravlev, V. A.; Minin, R. V.;Itin, V. I.;Lilenko, I. Y. Structural parameters and magnetic properties of copper ferrite nanopowders obtained by the sol-gel combustion. *Journal of Alloys and Compounds* **2017**, *692*, 705–712.
44. Prabhu, D.;Narayanasamy, A.; Shinoda, K.;Jeyadeven, B.; Greneche, J.-M.; Chattopadhyay, K. Grain size effect on the phase transformation temperature of nanostructured $CuFe_2O_4$. *Journal of Applied Physics* **2011**, *109*, 013532.

45. Dhyani, R.; Srivastava, R. C.; Rawat, P. S.; Dixit, G. Structural and elastic properties of tetragonal nano-structured copper ferrite. *International Journal of Materials Research* **2022**, *113*, 884-892.
46. Gingasu, D.; Mindru, I.; Patron, L.; Cizmas, C.-B. Tetragonal copper ferrite obtained by self-propagating combustion. *Journal of Alloys and Compounds* **2008**,*460*, 627–631.
47. Murthy, K. S. R. C.;Mahanty, S.; Ghose, J. Phase-transition studies on copper ferrite. *Materials Research Bulletin* **1987**, *22*, 1665–1675.
48. Tang, X.-X.;Manthiram, A.; Goodenough, J. B. Copper ferrite revisited. *Journal of Solid State Chemistry* **1989**, *79*, 250–262.
49. Tsoncheva, T.;Manova, E.;Velinov, N.;Paneva, D.; Popova, M.;Kunev, B.; Mitov, I. Thermally synthesized nanosized copper ferrites as catalysts for environment protection. *Catalysis Communications* **2010**, *12*, 105–109.
50. Tao, S.; Gao, F.; Liu, X.; Toft Sørensen, O. Preparation and gas-sensing properties of $CuFe_2O_4$ at reduced temperature. *Materials Science and Engineering: B* **2000**, 77, 172–176.
51. Desai, M.; Prasad, S.;Venkataramani, N.;Samajdar, I.; Nigam, A. K.; Krishnan, R. Cubic phase stabilization in sputter-deposited nanocrystalline copper ferrite thin films with large magnetization. *IEEE Transactions on Magnetics* **2002**, *38*, 3012–3014.
52. Caddeo, F.;Loche, D.; Casula, M. F.;Corrias, A. Evidence of a cubic iron sub-lattice in t-$CuFe_2O_4$ demonstrated by X-ray Absorption Fine Structure. *Scientific Reports* **2018**, *8*, 797.
53. Kester, E.;Gillot, B. Cation distribution, thermodynamic and kinetics considerations in nanoscaled copper ferrite spinels. New experimental approach by XPS and new results both in the bulk and on the grain boundary. *Journal of Physics and Chemistry of Solids* **1998**, *59*, 1259–1269.
54. Ohbayashi, K.; Iida, S. Oxygen Content and Thermomagnetic Properties in $Cu_{1-\varepsilon}Mg_{\varepsilon}Fe_2O_4$. *Journal of the Physical Society of Japan* **1967**, 23, 776–785.
55. Bergstein, A.; Červinka, L. To the structure and oxygen content of copper and copper-manganese ferrite. *Journal of Physics and Chemistry of Solids* **1961**, *18*, 264–265.
56. O'Bryan, H. M.;Levinstein, H. J.; Sherwood, R. C. Effect of Chemical Stoichiometry on the Copper Ferrite Phase Transition. *Journal of Applied Physics* **1966**, *37*, 1438–1439.
57. Phuruangrat, A.; Kuntalue, B.; Dumrongrojthanath, P.;Thongtem, T.;Thongtem, S. Microwave-assisted solvothermal synthesis of cubic ferrite (MFe_2O_4, M= Mn, Zn, Cu and Ni) nanocrystals and their magnetic properties. *Dig. J. Nanomater. Biostruct* **2018**, *13*, 563-568.
58. Gabal, M. A.;Katowah, D. F.; Hussein, M. A.; Al-Juaid, A. A.; Awad, A.; Abdel-Daiem, Saeed, A.; Hessien, M.M.; Asiri, A. M. Structural and Magnetoelectrical Properties of MFe_2O_4 (M = Co, Ni, Cu, Mg, and Zn) Ferrospinels Synthesized via an Egg-White Biotemplate. *ACS Omega* **2021**,6, 22180–22187.
59. Sung Lee, J.; Myung Cha, J.; Young Yoon, H.; Lee, J.-K.; Keun Kim, Y. (2015). Magnetic multi-granule nanoclusters: A model system that exhibits universal size effect of magnetic coercivity. *Scientific Reports* **2015**, 5.
60. Sumangala, T. P.; Mahender, C.;Barnabe, A.; Venkataramani, N.; Prasad, Structural, magnetic and gas sensing properties of nanosized copper ferrite powder synthesized by sol gel combustion technique. *Journal of Magnetism and Magnetic Materials* **2016**, 418, 48–53.
61. Mulud, F. H.; Dahham, N. A.;Waheed, I. F. Synthesis and Characterization of Copper Ferrite Nanoparticles. *IOP Conference Series: Materials Science and Engineering* **2020**, 928, 072125.